THE JOURNAL OF BIOLOGICAL CHEMISTRY VOL. 286, NO. 37, pp. 32563–32574, September 16, 2011

Severe Neurologic Impairment in Mice with Targeted Disruption of the Electrogenic Sodium Bicarbonate Cotransporter NBCe2 (*Slc4a5* Gene)*

Received for publication, April 13, 2011, and in revised form, June 23, 2011 Published, JBC Papers in Press, June 24, 2011, DOI 10.1074/jbc.M111.249961

Liyo Kao[‡], Lisa M. Kurtz[§], Xuesi Shao[¶], Marios C. Papadopoulos[‖], Li Liu[**], Dean Bok[¶‡‡§§], Steven Nusinowitz[‡‡], Bryan Chen[‡‡], Salvatore L. Stella[¶¶], Mark Andre[‡], Josh Weinreb[‡], Serena S. Luong[¶], Natik Piri[‡‡], Jacky M. K. Kwong[‡‡], Debra Newman[‡], and Ira Kurtz[‡§§1]

From the [‡]Department of Medicine, UCLA, Los Angeles, California 90095, the [§]Department of Neurosciences, University of California, San Diego, La Jolla, California 92093, the [¶]Department of Neurobiology, UCLA, Los Angeles, California 90095, the [‖]Academic Neurosurgery Unit, St George's University of London, London SW17 0RE, United Kingdom, the [**]Department of Pathology and Cell Biology, Columbia University Medical Center, New York, New York 10032, the [‡‡]Department of Ophthalmology, Jules Stein Eye Institute, UCLA, Los Angeles, California 90095, the [§§]Brain Research Institute, UCLA, Los Angeles, California 90095, and the [¶¶]Department of Basic Medical Science, University of Missouri-Kansas City, Kansas City, Missouri 64108

The choroid plexus lining the four ventricles in the brain is where the majority of cerebrospinal fluid (CSF) is produced. The secretory function of the choroid plexus is mediated by specific transport systems that allow the directional flux of nutrients and ions into the CSF and the removal of toxins. Normal CSF dynamics and chemistry ensure that the environment for neural function is optimal. Here, we report that targeted disruption of the *Slc4a5* gene encoding the electrogenic sodium bicarbonate cotransporter NBCe2 results in significant remodeling of choroid plexus epithelial cells, including abnormal mitochondrial distribution, cytoskeletal protein expression, and ion transporter polarity. These changes are accompanied by very significant abnormalities in intracerebral ventricle volume, intracranial pressure, and CSF electrolyte levels. The *Slc4a5*$^{-/-}$ mice are significantly more resistant to induction of seizure behavior than wild-type controls. In the retina of *Slc4a5*$^{-/-}$ mice, loss of photoreceptors, ganglion cells, and retinal detachment results in visual impairment assessed by abnormal electroretinogram waveforms. Our findings are the first demonstration of the fundamental importance of NBCe2 in the biology of the nervous system.

In the brain, normal neuronal activity and synaptic transmission require that intracellular and extracellular ion activity be maintained within narrow limits (1–3). Neurons and glia express various ion transporters that have evolved to ensure their normal function. The importance of these channels and transporters is highlighted by the abnormalities that result from human disease mutations and targeted gene disruption in animals, including sensorineural defects, decreased intelligence, seizures, paralysis, pain perception deficits, and ataxia (1, 4, 5). Neuronal function is also dependent on the maintenance of normal cerebrospinal fluid (CSF)[2] dynamics and composition (6). Approximately two-thirds of CSF is produced by choroid plexus epithelial (CPE) cells that express specific transport proteins, which mediate the directional transfer of water, ions, peptides, and organic molecules between blood and the CSF compartments (6, 7).

Modulating the production and chemistry of CSF is utilized clinically in the treatment of intracranial hypertension, mountain sickness, and seizure disorders (8–10) and would be of potential value in conditions such as Alzheimer disease (11, 12), normal pressure hydrocephalus (13), and aging (14), where the CSF turnover is abnormal leading to a buildup of harmful metabolites (6). The process of CSF transepithelial ion and fluid secretion involves an array of transporters and channels (6, 15). Fluid secretion is dependent on the active transepithelial transport of Na^+ mediated by an apical Na^+-K^+-ATPase pump, carbonic anhydrase activity, basolateral sodium bicarbonate influx mediated by the SLC4 transporter NCBE, and water transfer across the apical membrane via aquaporin 1. Additional ion transporters are expressed in CPE cells, including NBCn1, AE2, NHE1, Clir channels, NBCe2, VRAC, and NKCC1, which are also thought to play a role in CSF production (15).

NBCe2, an electrogenic sodium bicarbonate cotransporter belonging to the SLC4 family (16, 17), differs from other ion transport systems that are typically more widely expressed throughout the central nervous system in that it is localized to CPE cells (18, 19) and is therefore an interesting potential therapeutic target for modulating CSF production. In addition, whether alteration of the cotransporter function leads to a clinically relevant phenotype is also currently unknown. Therefore to determine whether NBCe2 plays a role in the maintenance of normal ventricular volume, intracranial pressure, and CSF chemistry, we generated mice with targeted disruption of the

* This work was supported, in whole or in part, by National Institutes of Health Grants DK077162 and DK058563 (to I. K.).

[1] To whom correspondence should be addressed: Dept. of Medicine and Brain Research Institute, Rm. 7-155 Factor Bldg., UCLA, Los Angeles, CA 90095-1689. E-mail: ikurtz@mednet.ucla.edu.

[2] The abbreviations used are: CSF, cerebrospinal fluid; PTZ, pentylenetetrazole; ICP, intracranial pressure; CPE, choroid plexus epithelial; RGC, retinal ganglion cell; ERG, electroretinogram; IOP, intraocular pressure; ROS, rod outer segment; ONL, outer nuclear layer; RPE, retinal pigment epithelium; OPL, outer plexiform layer; NCBE, sodium-driven chloride bicarbonate exchanger.

Slc4a5 gene. Our findings show that loss of NBCe2 results in severe brain ventricular hypovolemia and decreased intracranial pressure. Unexpectedly, the mice also developed a severe retinopathy demonstrating, for the first time, the biologic importance of NBCe2 in visual sensori-neural transduction in the mammalian retina.

EXPERIMENTAL PROCEDURES

Generation of Slc4a5$^{-/-}$ Mice—The UCLA Animal Subject Protection Committee approved the research protocols used for the mice studies. The mice were cared for and handled in accordance with the Animal Welfare Act and in strict compliance with guidelines from the National Institutes of Health. Mice deficient for *Slc4a5*$^{-/-}$ were generated by infecting embryonic stem cells (129/SvEv^{Brd}) with the retroviral gene trap vector VICTR48 (Lexicon Genetics), which integrated upstream of exon 15 (Fig. 1, *A* and *B*). The vector contains the following: 1) a splice acceptor, followed downstream by a neomycin resistance gene and polyadenylation sequence, and 2) stop codons in all three reading frames, preventing gene expression by terminating translation (20, 21). The disrupted *Slc4a5* gene in an embryonic stem cell line was injected into C57BL/6J blastocysts. The blastocysts were then implanted in pseudopregnant females, and offspring were crossed with C57BL/6J mice. The animals were genotyped by PCR. Heterozygotes were bred to homozygosity and subsequently used for genetic and phenotypic analysis. NBCe2 protein was detected in the choroid plexus and retina from wild-type mice, whereas no protein was detected from *Slc4a5*$^{-/-}$ mice (see below). Littermate controls were utilized for comparison experiments.

Genotyping—Genomic DNA from mice tails was isolated using the GenElute mammalian genomic DNA miniprep kit (Sigma) according to the manufacturer's protocol. The following primer pairs were used to detect the wild-type alleles (product size 591 bp): 5′-AATAGCCTCCAAGGACCTTAGCTGC-3′ and 5′-AATGTAAAGACAGACCAAAGCATCC-3′. Mutant alleles were detected with the following primers (product size 352 bp): 5′-AATGTAAAGACAGACCAAAGCATCC-3′ and 5′-AAATGGCGTTACTTAAGCTAGCTTGC-3′.

Immunoblotting of the Choroid Plexus and HEK-293 Cells—Choroid plexus wild-type and *Slc4a5*$^{-/-}$ mice were dissected from the fourth ventricle and suspended in 500 μl of lysis solution (50 mM Tris·HCl, pH 7.5) with complete Mini protease inhibitor mixture (1 tablet/2 ml, Roche Applied Science) and 1 μg/ml pepstatin and then disrupted in a glass homogenizer. The homogenate was then passed 40 times through a 25-gauge needle (BD Biosciences), centrifuged at 600 × *g* for 10 min, and processed for immunoblotting. In separate experiments, HEK-293 cells transiently expressing NBCe2 using Lipofectamine 2000 (Invitrogen) were prepared for immunoblotting using the same protocol. Protein samples were resolved on 7.5% polyacrylamide gels and transferred to polyvinylidene difluoride membranes. Protein expression was assessed by probing the blot with the anti-NBCe2 rabbit polyclonal antibody (targeted against the mouse C-terminal sequence MEGIPSDPQNGIHC (Bethyl Laboratories Inc., Montgomery, TX) at 1:3,000 dilution in TBSTM buffer (0.1% (v/v) Tween 20, 137 mM NaCl, 20 mM Tris, pH 7.5, containing 5% (w/v) nonfat milk).

Immunohistochemistry of the Choroid Plexus and Retina—The animals were anesthetized with isofluorane and cardiac-perfused with 10% formalin (Thermo Fisher Scientific Inc., Waltham, MA) for 10 min. For immunohistochemistry of the choroid plexus, the brain was removed and sectioned, and coronal sections were cryoprotected in 25% sucrose overnight at 4 °C. The tissue was infiltrated with Tissue-Tek OCT compound (Sakura Finetek Inc., Torrance, CA), rapidly frozen, and 5-μm cryostat sections were cut and mounted on Superfrost plus glass slides (Fisher) and stored at −80 °C. The following antibodies were used: NBCe2 (Bethyl Laboratories Inc); Na^+-K^+-ATPase α1 subunit (Millipore, Billerica, MA); aquaporin 1 (Abcam Inc., Cambridge MA); aquaporin 4 (Santa Cruz Biotechnology, Inc., Santa Cruz, CA), NHE1 (Abcam Inc); NKCC1 (Abcam Inc); Na^+-K^+-ATPase β1 and β2 subunits (gift from Alicia Mcdonough); NBCn1 (gift from Soren Nielsen); NCBE (Bethyl Laboratories Inc); AE2 (Abcam Inc), and spectrin βII (Santa Cruz Biotechnology). All primary antibodies were diluted in PBS (1:10–1:100) and incubated for 30 min at room temperature. After washing in PBS, the slides were incubated for 30 min with either secondary goat anti-rabbit Alexa 488 (NCBE), goat anti-rabbit Alexa 594 (NBCe2, aquaporin 1, aquaporin 4, NHE1, NBCn1, and Na^+-K^+-ATPase β1 and β2 subunits) or goat anti-mouse Alexa 488 (Na^+-K^+-ATPase α1 subunit, spectrin βII). In the eye studies, the ora serrata, cornea, lens, and vitreous body were removed, and the eyecups were immersion-fixed in 4% paraformaldehyde in PBS for 15–30 min at room temperature. The eyes were then cryoprotected in 25% sucrose overnight at 4 °C. Prior to cutting the tissue with a cryostat, the retina was washed with PBS and embedded in Tissue-Tek OCT compound and rapidly frozen with dry ice or liquid nitrogen. Cryostat sections of the retina were cut at 12–15 μm, mounted onto gelatin-coated slides, air-dried, and stored at −20 °C until staining with the anti-NBCe2 antibody (1:100) and (secondary goat anti-rabbit Alexa 488, 1:500). Fluorescent images were acquired using a Zeiss 510 META laser scanning microscope (Zeiss, Thornwood, NY).

Histology of the Choroid Plexus, Light and Electron Microscopy—The mice were anesthetized with isofluorane and cardiac-perfused for 10 min using 2% formaldehyde and 2.5% glutaraldehyde (Ted Pella Inc., Redding, CA) in 0.1 M sodium phosphate buffer, following which the brain was removed and left in the fixative overnight at 4 °C. The formaldehyde was made fresh from paraformaldehyde (EM Grade, Ted Pella). The tissue was then washed with serial ethanol dilutions (70, 80, 95, and 100%, two each), two times in xylene, three times in paraffin, and embedded in paraffin blocks. The brains were sectioned in the horizontal orientation starting from the dorsal side at a thickness of 5 μm, mounted on positively charged slides, and H&E-stained. The sections were coverslipped, and digital photomicrographs of sections were obtained using a ScanScope XT system (Aperio Technologies, Inc., Vista, CA) at a magnification of ×40.

For electron microscopy, the brain was infiltrated with 1:1 Epon and acetone for 30 min and then infiltrated with 3:1 Epon and acetone for 45 min. The brain was then placed into 100%

EPON for 1 h and then embedded in molds and polymerized in a 70–75 °C oven for 48 h. Once the blocks were fully polymerized, 1-μm sections were stained with toluidine blue O or methylene blue. Once a specific area was selected for further examination, ultrathin sections of ~90 nm were obtained using a RMC MT Ultramicrotome. Sections were collected on copper EM grids, and the grids were stained with uranyl acetate and lead stain. Grids were examined with a Philips EM208S electron microscope, and digital images were obtained with an attached AMT digital camera.

Histology of the Retina, Light and Electron Microscopy—Following isofluorane anesthesia, the mice were cardiac-perfused as described above. The eye was removed, put into 1% osmium tetroxide for 1 h, and then rinsed again three times for 10 min; each rinse was in cold distilled water (4 °C). The eye was then dehydrated in a series of cold ethanol (4 °C) (50, 70, 95, and 100%), infiltrated with propylene oxide three times for 10 min each, and then left overnight in a solution of equal parts monomer (Epon/araldite + dodecenyl succinic anhydride with 2% DMP-30) to propylene oxide. The next day the eye was placed in freshly prepared pure monomer resin for 1 h, then embedded in BEEM capsules, and placed in the 80 °C oven for 6 h. Once the blocks were fully polymerized, the tissues were sectioned at 1 μm with a Leica Ultracut UCT ultramicrotome. Sections were collected on clean glass slides and stained with 1% toluidine blue containing 1% sodium borate. For the retinal sections, digital images were taken with a Zeiss Axiophot microscope with attached Coolsnap Pro digital camera with a ×63 oil immersion objective lens.

For electron microscopy at the end of the propylene oxide infiltration step (as described above), the eye was infiltrated with one part araldite to two parts propylene oxide for 30 min on a rotator. The eye was then infiltrated with two parts araldite to one part propylene oxide for 30 min on the rotator. The eye was placed in into pure araldite for 1 h and then embedded in flat embedding molds in the 60 °C oven for 48 h. Once the blocks were fully polymerized, the tissue was cut using a Leica Ultracut UCT ultramicrotome to cut 90-nm ultrathin sections. Sections were collected on copper EM grids, and the grids were stained with 5% uranyl acetate and 0.4% lead citrate. Digital images were taken with a Zeiss EM910 electron microscope with attached Keenview digital camera.

Optic Nerve Injury Evaluation and Retinal Ganglion Cell (RGC) Quantitation—Animals were anesthetized by intramuscular injection of Nembutal at 85 mg/kg (sodium pentobarbital 50 mg/ml; Ovation Pharmaceutical, Inc., Deerfield, IL) and transcardially perfused with 4% paraformaldehyde. After enucleation, the retinas were immediately dissected and fixed with 4% paraformaldehyde in 0.1 M phosphate buffer for 1 h. The retinas were washed with PBS and processed for whole retina immunohistochemistry according to Kong and Cho (22) with minor modifications. Briefly, the retinas were incubated with 10% fetal bovine serum for 1 h to block nonspecific staining and then primary antibody against the previously characterized RGC marker, Rbpms (23), (1:500) in PBS containing 1% Triton, 0.5% BSA, and 0.9% sodium chloride (PBS-T/BSA) overnight at 4 °C. Following incubation with secondary Alexa Fluor 488 goat anti-rabbit IgG antibody (1:1,000) overnight at 4 °C, the retinas were washed with PBS. The retinas were divided into four quadrants: superior-temporal, superior-nasal, inferior-temporal, and inferior-nasal. One sampling field (0.32 × 0.24 mm each) was collected at each region of 0.5, 1, 1.5, and 2 mm from the center of the optic nerve in each retinal quadrant by fluorescent microscopy (LSM410, Carl Zeiss, Oberkochen, Germany). The number of RGCs in 16 sampling fields from each retina was counted and analyzed. Morphometric analysis of each optic nerve was performed as described previously (24). In brief, after perfusion, 2-mm segments of optic nerve were obtained starting 1 mm behind the globe. These segments of optic nerve were fixed by immersion in 2% glutaraldehyde and 1% paraformaldehyde for 24 h at 4 °C, processed, and embedded in acrylic resin. Optic nerve cross-sections (1 μm thick) were stained with a solution of 1% toluidine blue and examined under light microscopy and assessed by two independent masked observers.

Patch Clamp Recordings of Choroid Plexus—Choroid plexus was dissected from the fourth ventricle and stabilized on the bottom of tissue culture dishes by a threaded frame. Cells were continually superfused at room temperature with bath solution (~2 ml/min) containing (in mM) sodium aspartate 133.5, cesium aspartate 10, $CaCl_2$ 1.5, $MgCl_2$ 1.0, HEPES 10, glucose 15, pH 7.3. Cells were whole-cell patch-clamped using a patch clamp amplifier (MultiClamp 700B, Molecular Devices) and with IR-DIC microscope (Axioskop2, Carl Zeiss, Göttingen, Germany). Patch pipettes were pulled from a thick wall (0.32 mm) of borosilicate glass with a tip size of 1–1.5 μm (resistance of 4–7 megohms). The patch pipette filling solution contained cesium gluconate 130, sodium gluconate 5, $MgCl_2$ 1.0, $CaCl_2$ 1.0, EGTA 10, HEPES 10, pH 7.3. To ensure stable electrode potentials during patch clamp recordings, a micro-agar salt bridge of 2 M KCl was built in the electrode holder that formed an electrical connection between the pipette solution and the Ag/AgCl wire connected to the headstage of a patch clamp amplifier (25). Whole-cell capacitance and series resistance were determined with the auto whole-cell capacitance and series resistance compensation in the MultiClamp 700B. The series resistance was usually compensated at 80%. Patch pipette junction potential was determined with the junction potential calculator in software Clampex 10 (Molecular Devices); the reported potential values were corrected for junction potentials. Signals from whole-cell patch recordings were low pass-filtered at 400 Hz and digitized at a 2-kHz sampling frequency with a Digidata 1440A and Clampex 10 software (Molecular Devices). The signals were saved as data files for further analyses off-line.

Brain NMR Imaging—The mice were anesthetized using isoflurane and maintained by monitoring temperature and respiration and imaged using a Biospec 70/30 7 Tesla magnet 7T scanner (Bruker Biospin, Germany). T2-weighted scout images were made in axial, coronal, and sagittal orientations. High resolution T2-weighted two-dimensional MSME (multispin multiecho) (three-echo sequence, echo time = 30, 60, and 90 ms, repetition time = 3,000 ms, averages = 3, 20 coronal slices = 20, slice thickness = 350 nm, matrix = 256 × 128, field of view = 4.0 × 2.0 cm, acquisition time = 19 min, 12 s) were acquired based on the scout images. To indirectly assess brain

water content, T2 relaxations times were measured from an analysis of the multiecho images in various brain regions. Single echo volumes were extracted from using MIPAV software, and a three-dimensional analysis was performed using MRIcro program after converting the volume into isometric voxels. The ventricular CSF compartment in each image was highlighted, and the volume of the highlighted region was calculated automatically by multiplying the number of voxels by the volume of each voxel. The volumes of all the highlighted regions were summed to determine the entire ventricular volume.

ICP Measurement—Mice were anesthetized using 2.5% 2,2,2-tribromoethanol (Avertin, Sigma) by injecting intraperitoneally a 6.7 ml/kg bolus followed by 1.7 ml/kg every 20 min. The mice were immobilized in a stereotactic frame (myNeurolab, St. Louis, MO). Rectal temperature was maintained at 37–37.5 °C using a heat lamp. A midline scalp incision was made, and a 0.8-mm diameter burr hole was drilled using a Foredom drill (Bethel, CT), 2 mm to the right and 2 mm behind the bregma. An ICP monitoring micro-probe (SPC-320; 0.6 mm diameter; Millar, Houston, TX) was inserted intraparenchymally 2 mm deep from the brain surface. ICP recordings were taken at a rate of 100 Hz using a computer interface (MP 35; Biopac, Santa Barbara, CA). The ICP was monitored for 4 min. The first 2 min of recording was discarded, and the ICP readings corresponding to the last 2 min were averaged.

Brain Water Content—The mice were sacrificed, and the brain was rapidly removed and divided into right and left cerebral hemispheres and cerebellum. Each brain fragment was weighed immediately, dried in an oven (90 °C, 48 h), and reweighed. Percent brain water content was computed as 100 × (wet weight − dry weight)/wet weight.

CSF Electrolytes—Mice were anesthetized intraperitoneally with Ketamine (100 mg/kg) and xylazine (10 mg/kg) and maintained 37 °C. To collect CSF, a capillary tube was inserted into the cisterna magna through the dura mater, lateral to the arteria dorsalis spinalis. The CSF was injected into an Eppendorf tube and frozen immediately on dry ice. CSF Na^+, K^+, and TCO_2 were measured using a Vitros 250 chemistry analyzer (Johnson & Johnson Co., New Brunswick, NJ).

Seizure Behavior—PTZ (45 mg/kg; Sigma) was injected intraperitoneally into mice 3–6 months of age. Following injection, the mice were placed into a clear plastic box, and their behavior was monitored by video recording for 20 min. Seizure activity was subsequently analyzed and classified according to the duration and degree of generalization as described previously (26) and as follows: stage 0, no response; stage 1, facial twitching; stage 2, myoclonic jerks without upright position; stage 3, myoclonic jerks and upright position with bilateral forelimb clonus; stage 4, clonic-tonic seizures; stage 5, generalized clonic-tonic seizures with loss of postural control. Intensity of seizure activity was scored by assigning a numerical value equal to the highest stage level that was detected in a given trial.

Electroretinography—Mice, dark-adapted overnight, were anesthetized with an intraperitoneal injection of normal saline containing ketamine (15 μg/gm) and xylazine (7 μg/g body weight). Electroretinograms (ERGs) were recorded from the corneal surface of one eye after pupil dilation (1% atropine sulfate) using a gold loop electrode referenced to a similar gold wire in the mouth. A needle electrode in the tail served as ground. A drop of methylcellulose (2.5%) on the corneal surface was used to ensure electrical contact and to maintain corneal integrity. Body temperature was maintained at 38 °C with a heated water pad. Mice were positioned in front of an opening cut into a large dome (LKC Technologies) whose interior surface was painted with a highly reflective white matte paint (Eastman Kodak Corp., catalog 6080). All stimuli were generated with a Grass Photic Stimulator (Grass Instruments, PS33 Plus) affixed to the outside of the dome at 90° to the viewing porthole. Responses were amplified (Grass CP511 AC amplifier, x10,000) and digitized using a I/O board (National Instruments, PCI-1200) in a personal computer. Signal processing was performed with custom software (National Instruments, LabWindows/CVI). For each stimulus condition, responses were computer-averaged with up to 50 records averaged for the weakest signals. Rod responses were recorded to blue (Wratten 47A; $\lambda max = 470$ nm) flashes of light over a 4.0 log unit range of intensities (in 0.3 log unit steps) up to the maximum allowable by the photic stimulator (0.35 cd/m^2). Cone responses were obtained with white flashes on the rod-saturating background (32.0 cd/m^2) after 10 min of exposure to the background light to allow complete light adaptation.

Spectral Domain Optical Coherence Tomography (SD-OCT)—Animals were anesthetized with a 6:3:1 solution of balanced salt solution, ketamine (100 mg/ml), and xylazine (20 mg/ml). Injections were performed intraperitoneally, and doses contained 4 μl of anesthetic/g of body weight. 1 drop of a 1:1 mixture of 2.5% phenylephrine and 1% tropicamide ophthalmic solution was used to dilate pupils. SD-OCT imaging was performed on the right eye of each animal with a commercially available three-dimensional SD-OCT system equipped with an 840 nm superluminescent LED light source (Bioptigen, Research Triangle Park, NC). Recordings were taken with a 50° field of view, yielding a 1.5-mm diameter image. *En face* view C-scans were recorded with the optic nerve head centered in the image, which consisted of 100 two-dimensional B-scans, which in turn consisted of 800 one-dimensional A-scans. A higher resolution B-scan in the plane of the optic nerve head was also taken by averaging 5 B-scans together with 1000 A-scans per B-scan. Retinal layers were measured in the plane of the optic nerve head with analysis software (Software Suite, Bioptigen).

Intraocular Pressure—Intraocular pressure (IOP) measurements were obtained with the Tonolab tonometer (Colonial Medical Supply, Franconia, NH), a rebound tonometer designed specifically for rodents. Mice were anesthetized as described above (ERG protocol) and positioned on a movable platform that permitted precise positioning of the mouse eye. In addition, the tonometer was attached to an X,Y,Z-movable stage so that the probe tip (Small Animal Probe; Tiolat Finland Oy, Finland) could be positioned exactly 2 mm from the corneal surface of the eye. A calibration table for the mice was provided by the manufacturer. The TonoLab recorded six measurements deemed reliable by internal software and then generated and displayed an average of these measurements.

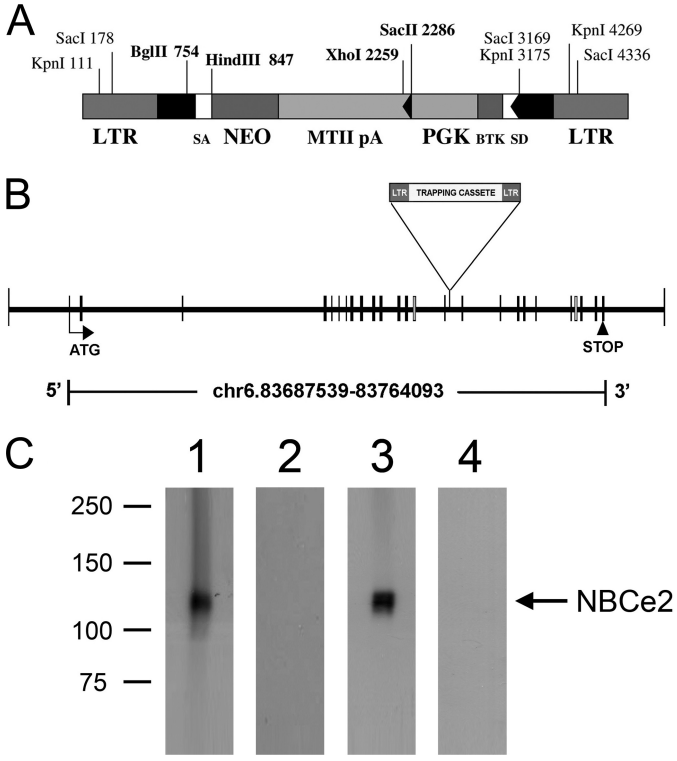

FIGURE 1. **Insertional deletion of *Slc4a5*.** *A*, restriction map of the retroviral gene trap vector, VICTR48. *B*, structural arrangement of 129 Sv/Ev^{brd} mouse gene *Slc4a5*; diagram of the mutated *Slc4a5* allele after insertion. *LTR*, long terminal repeat. *C*, Western analysis. *Lane 1*, wild-type choroid plexus labeled with the NBCe2 antibody; *lane 2*, *Slc4a5*$^{-/-}$ choroid plexus showing lack of labeling with the NBCe2 antibody; *lane 3*, HEK-293 cells expressing NBCe2 labeled with the NBCe2 antibody; *lane 4*, HEK-293 cells expressing NBCe2 labeled with the NBCe2 antibody preincubated with the immunizing peptide.

Statistical Analysis—Mann Whitney *U* test was used to assess statistical significance with $p < 0.05$ considered significant. Results are reported as mean ± S.E.

RESULTS

Loss of CPE Cell Expression of NBCe2, Abnormal Morphology and Ultrastructural Changes—The choroid plexus of *Slc4a5*$^{-/-}$ mice does not express NBCe2 (Figs. 1*C* and 2, *A–C*) and lacks electrogenic NBCe2-mediated ion flux (Fig. 2, *D* and *E*). As shown in Fig. 3, *A* and *B*, the choroid plexus (dissected from the fourth ventricle) had protrusions that were not detected in wild-type mice. Morphologically, choroid plexus epithelial cells from *Slc4a5*$^{-/-}$ mice appeared abnormal. The cells were less columnar and had a more granular cytoplasm (Fig. 3, *C* and *D*). Ultrastructurally, mitochondria that are typically apically located in CPE cells were more evenly distributed throughout the cytoplasm in mice lacking NBCe2 (Fig. 3, *E* and *F*).

Survey of H^+/Base and Ion Transporters in CPE Cells, Altered Expression Pattern—The morphologic and ultrastructural changes in CPE cells lacking NBCe2 suggested that a more global cellular remodeling abnormality is present. We therefore next examined the localization of H^+/base transporters that are normally expressed on either the apical or basolateral membrane in CPE cells. Specifically, the expression pattern of AE2 (basolateral Cl^--bicarbonate exchanger (27)), NBCn1 (apical or basolateral electroneutral sodium bicarbonate cotransporter depending on mouse strain (28)), NHE1 (apical Na^+/H^+ exchanger (28)), and NCBE (basolateral Na^+-driven Cl^--bicarbonate exchanger (29)), were examined as is shown in Fig. 4. Significant changes were observed in the localization of NCBE

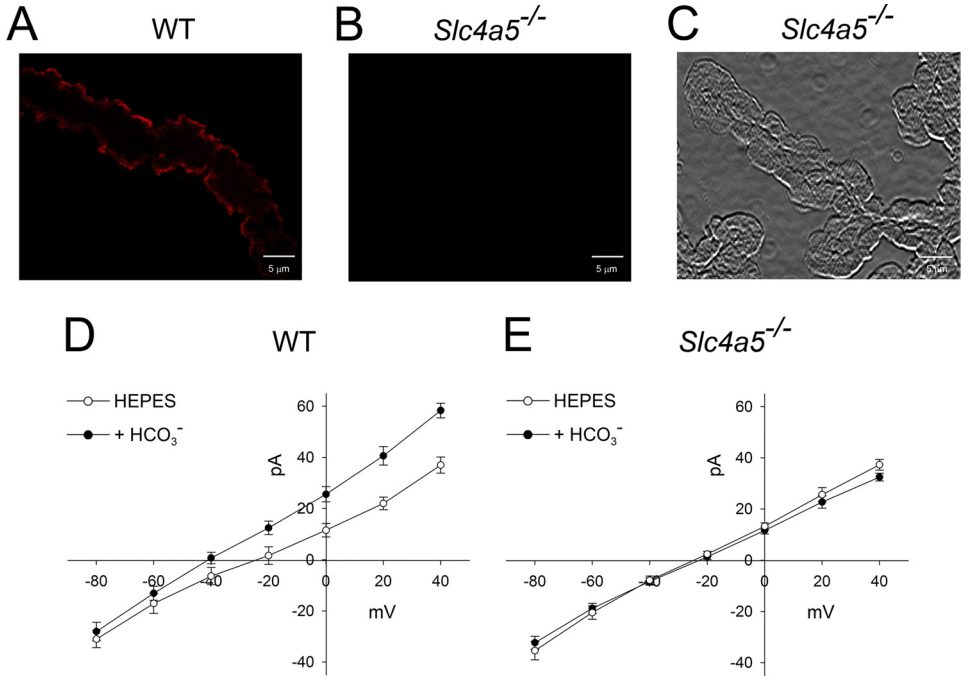

FIGURE 2. *A*, immunolocalization of NBCe2 in wild-type CPE cells. *B*, CPE cells from *Slc4a5*$^{-/-}$ mice fail to express NBCe2. *C*, Nomarski image corresponding to the immunofluorescence image shown in *B*. *D* and *E*, function of NBCe2 in wild-type CPE cells ($n = 4$) and lack of function in *Slc4a5*$^{-/-}$ CPE cells ($n = 6$). A series of 400-ms voltage clamp pulses ranging from −80 to +40 mV with an increment of 20 mV was applied, and whole-cell current responses were recorded. Current-voltage (*I-V*) relationship of steady-state current in the absence and presence of HCO_3^- is presented. The results show that only wild-type CPE cells generate a positive current because of NBCe2-mediated transport in the presence of bicarbonate.

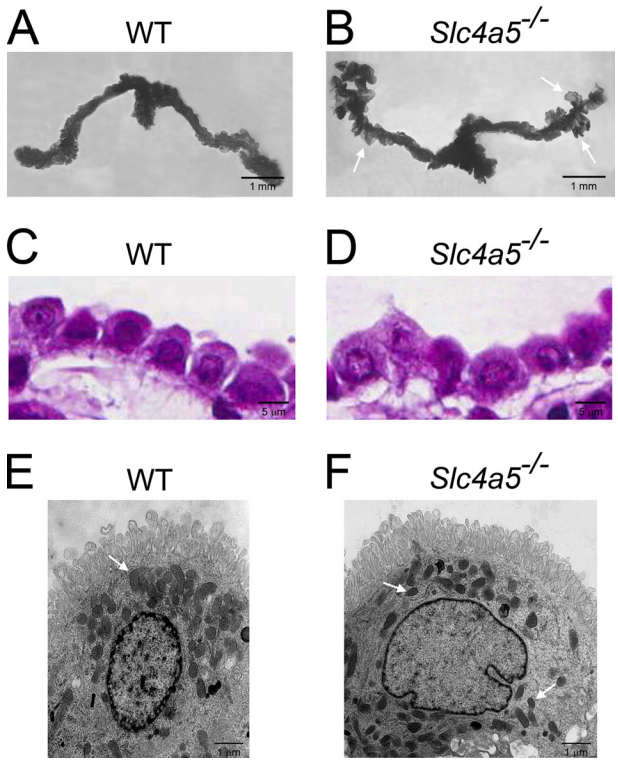

FIGURE 3. **Dissected fourth ventricle choroid plexus.** *A,* wild-type mice; *B, Slc4a5*$^{-/-}$ mice. The choroid plexus from *Slc4a5*$^{-/-}$ mice have protrusions (*arrows*) that were not seen in control mice. Morphology of CPE cells (H&E stained cells) from wild-type mice (*C*) and *Slc4a5*$^{-/-}$ mice (*D*) is shown. Cells from *Slc4a5*$^{-/-}$ mice appear less columnar and have a granular cytoplasmic appearance. *E,* electron micrograph image of a CPE cell from wild-type mice showing apically localized mitochondria (*arrow*) in comparison with a cell from *Slc4a5*$^{-/-}$ mice (*F*) where the mitochondria (*arrows*) are more evenly dispersed.

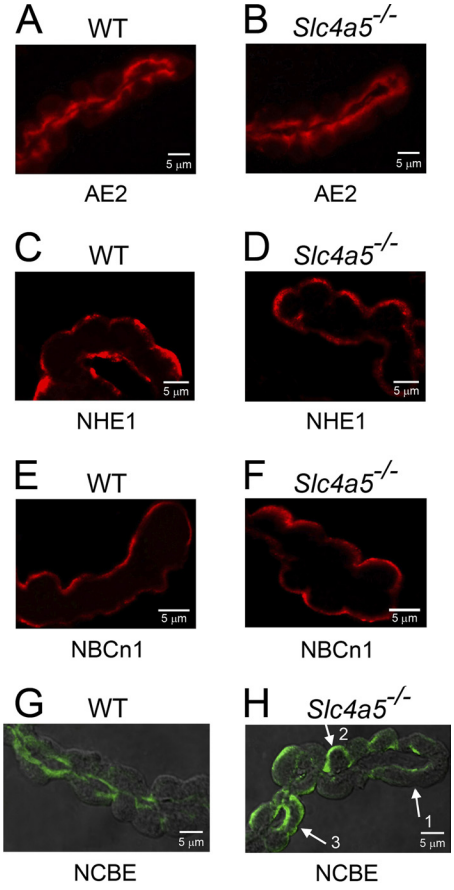

FIGURE 4. **Immunolocalization of H$^+$/base transporters in CPE cells from wild-type and *Slc4a5*$^{-/-}$ mice.** *AE2*, wild-type (*A*); *Slc4a5*$^{-/-}$ (*B*); *NHE1*, wild-type (*C*); *Slc4a5*$^{-/-}$ (*D*); *NBCn1*, wild-type (*E*), *Slc4a5*$^{-/-}$ (*F*); *NCBE*, wild-type (*G*), *Slc4a5*$^{-/-}$ (*H*). Unlike wild-type CPE cells, which express NCBE basolaterally, in *Slc4a5*$^{-/-}$ CPE cells, the transporter is localized basolaterally (*1*), apically (*2*), or bilaterally (*3*).

(Fig. 4, *G* and *H*), which normally mediates basolateral sodium bicarbonate influx in CPE cells. NCBE is normally localized on the basolateral membrane; however, in *Slc4a5*$^{-/-}$ mice, the transporter was expressed in CPE cells on either the apical membrane, the basolateral membrane, or bilaterally.

In addition to changes in the pattern of NCBE expression, as shown in Fig. 5, CPE cells from *Slc4a5*$^{-/-}$ mice had an altered expression pattern of Na^+ pump subunits, NKCC1, and the spectrin βII cytoskeleton protein. In CPE cells lacking NBCe2, the Na^+ pump α1 subunit, which is normally localized apically (30), was expressed bilaterally (Fig. 5, *A* and *B*). There was no change in the apical expression (31) of the β1 subunit (Fig. 5, *C* and *D*), yet the β2 subunit, which is normally expressed apically (31), was undetectable (Fig. 5, *E* and *F*). In several CPE cells, NKCC1 was detected intracellularly, and in other cells the cotransporter was apically expressed as in wild-type cells (Fig. 5, *G* and *H*) (32). This array of changes in mitochondrial distribution, ion transporter, and cytoskeletal expression highlight the previously unknown requirement for NBCe2 in the normal cellular modeling of CPE cells.

Decreased CSF Ventricular Volume, Intracranial Pressure—We next examined whether the cellular changes resulting from the absence of NBCe2 is associated *in vivo* with changes in CSF volume and pressure. As shown in Fig. 6, *A* and *B*, NMR imaging studies in *Slc4a5*$^{-/-}$ mice demonstrated that the volume of the lateral ventricles was significantly abnormal. In wild-type mice, the mean volume was 6.58 ± 0.58 mm^3 ($n = 6$), and in the *Slc4a5*$^{-/-}$ mice, the mean volume was 1.79 ± 0.28 mm^3 ($n = 6$) $p < 0.05$. The water content of the cerebrum and cerebellum was unchanged (~77 and ~74%, respectively) in wild-type and *Slc4a5*$^{-/-}$ mice. These findings were corroborated by NMR T2 relaxation time analysis, which did not show any differences among the mice in various brain regions (data not shown). In addition to decreased ventricular volume, *Slc4a5*$^{-/-}$ mice had a significant decrease in ICP as follows: 9.22 ± 1.35 cm H_2O ($n = 5$) *versus* 2.98 ± 0.67 cm H_2O ($n = 5$) $p < 0.05$ (Fig. 6, *C* and *D*). These changes were not accompanied by alterations in the expression pattern of the aquaporin 1 (Fig. 6, *E* and *F*) and aquaporin 4 water channels (Fig. 6, *G* and *H*). Our data demonstrate for the first time an essential role for NBCe2 in the maintenance of normal CSF ventricular volume and pressure.

Abnormal CSF Electrolytes—The question as to whether the loss of NBCe2 that results in decreased ventricular volume and intracranial pressure is also associated with changes in the CSF Na^+, HCO_3^- and K^+ concentration was next studied. Two possibilities are apparent. 1) The decrement in water flux and electrolyte flux is in proportion and is not associated with changes in CSF electrolyte concentrations. 2) The changes in ion and water flux are not in proportion resulting in changes in CSF ion chemistry. In wild-type mice, the CSF Na^+ concentration was

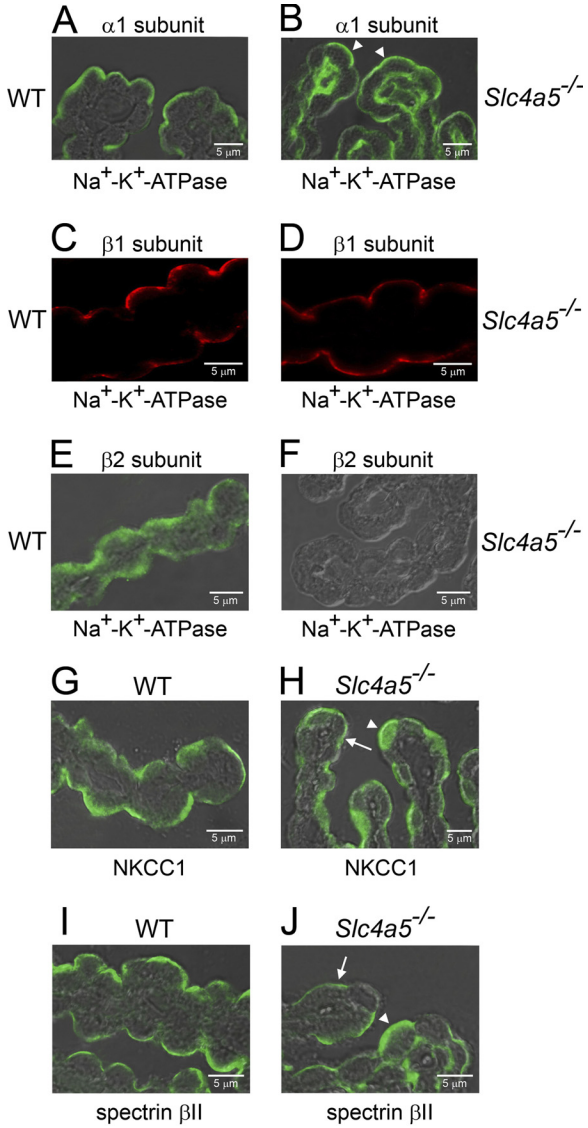

FIGURE 5. **Immunolocalization of Na^+ pump subunits, NKCC1 and spectrin *βII* cytoskeleton protein.** α1 Na^+ pump subunit is expressed apically in wild-type CPE cells (*A*) and bilaterally (*arrowhead*) in CPE cells from *Slc4a5*$^{-/-}$ mice (*B*). The β1 Na^+ pump subunit was expressed apically in both wild-type (*C*) and *Slc4a5*$^{-/-}$ CPE cells (*D*). Unlike wild-type CPE cells (*E*), CPE cells from *Slc4a5*$^{-/-}$ mice fail to express the β2 Na^+ pump subunit (*F*). NKCC1 that is expressed apically in wild-type CPE cells (*G*) is localized apically (*arrow*) and apically + intracellularly (*arrowhead*) in CPE cells from *Slc4a5*$^{-/-}$ mice (*H*). Apical localization of spectrin βII in wild-type CPE cells (*I*) compared with its apical (*arrow*) and bilateral (*arrowhead*) expression in CPE cells from *Slc4a5*$^{-/-}$ mice (*J*).

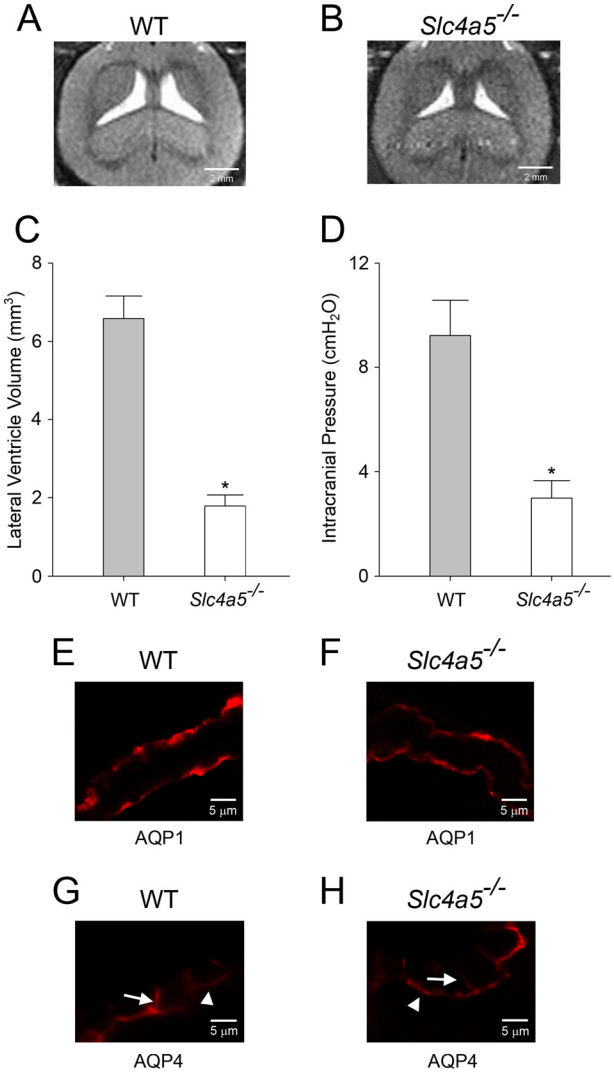

FIGURE 6. MRI imaging (horizontal plane) of the lateral ventricles in wild-type (*A*) and *Slc4a5*$^{-/-}$ mice (*B*) is shown. *C*, lateral ventricle volume assessed using MIPAV software and a three-dimensional analysis was performed using the MRIcro program. The ventricular volume in *Slc4a5*$^{-/-}$ mice was significantly reduced; *, $p < 0.05$. *D*, intracranial pressure was also significantly reduced in *Slc4a5*$^{-/-}$ mice; *, $p < 0.05$. Aquaporin 1 expression was unchanged in CPE cells from wild-type (*E*) *versus* *Slc4a5*$^{-/-}$ mice (*F*). Similarly, aquaporin 4 expression was unchanged in wild-type (*G*) *versus* *Slc4a5*$^{-/-}$ (*H*) ventricular ependymal cells.

not significantly different from *Slc4a5*$^{-/-}$ mice: 162 ± 1 meq/liter (n = 11) *versus* 160 ± 1 meq/liter (n = 11), respectively, p = not significant. In contrast, the CSF HCO_3^- concentration was significantly decreased from 24 ± 1 meq/liter (n = 14) to 20 ± 1 meq/liter (n = 11) in *Slc4a5*$^{-/-}$ mice, $p < 0.05$. The CSF K^+ concentration was significantly increased in *Slc4a5*$^{-/-}$ mice as follows: 3.6 ± 0.1 meq/liter (n = 7) to 4.7 ± 0.1 meq/liter (n = 12), $p < 0.05$. These findings represent the first reported measurements of changes in CSF ion chemistry because of loss of a choroid plexus transporter.

Decreased Seizure Behavior Propensity in Slc4a5$^{-/-}$ *Mice*—Changes in CSF chemistry and pressure are associated with alterations in neuronal excitability (6). Furthermore, acetazolamide, an inhibitor of carbonic anhydrase activity and choroid plexus bicarbonate transport, has been used clinically to decrease intracranial pressure and as a therapy for seizures (33, 34). We therefore tested the whether seizure susceptibility of *Slc4a5*$^{-/-}$ mice given the chemoconvulsant PTZ differed from wild-type mice. Mice were administered PTZ at a dose of 45 mg/kg PTZ intraperitoneally. The seizure score in wild-type mice was 4.50 ± 0.34 (n = 6) compared with 2.33 ± 0.34 (n = 6) in *Slc4a5*$^{-/-}$ mice, $p < 0.05$. These results demonstrate that *Slc4a5*$^{-/-}$ mice have a significantly lower susceptibility to chemically induced seizure behavior.

Ocular Functional and Morphologic Abnormalities in Slc4a5$^{-/-}$ *Mice—Slc4a5*$^{-/-}$ mice had significant visual abnormalities. As shown in Fig. 7, *A–C*, SD-OCT studies demonstrate retinal detachment of varying severity, and functional ERG studies reveal abnormal wave amplitudes (Fig. 7, *D* and *E*).

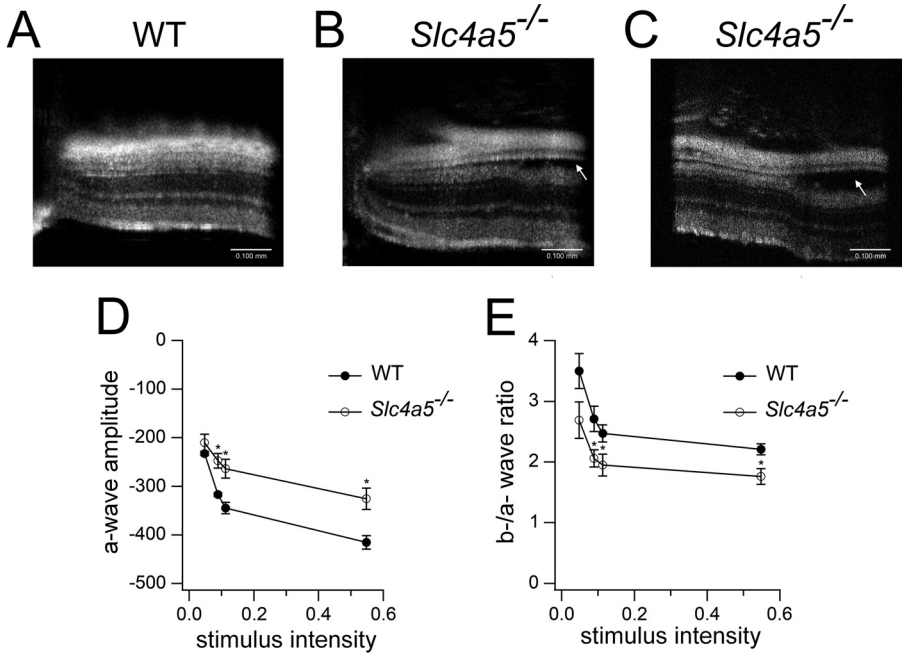

FIGURE 7. *A–C,* SD-OCT studies of wild-type (*A*) and *Slc4a5*$^{-/-}$ (*B* and *C*) retinas. *Slc4a5*$^{-/-}$ had retinal detachment of varying severity (*B* and *C*). *D,* ERG studies in wild-type and *Slc4a5*$^{-/-}$ mice are as follows: *a*-wave amplitude (mean ± S.E.) as a function of stimulus intensity for wild-type mice (*filled symbols*) and *Slc4a5*$^{-/-}$ mice (*open symbols*). These findings are consistent with the observations on EM of diminished photoreceptor number, shorter and dysmorphic outer segments, and inappropriate apposition of the photoreceptor outer segment tips with the RPE in *Slc4a5*$^{-/-}$ mice; *, $p < 0.05$. *E,* ERG studies in wild-type and *Slc4a5*$^{-/-}$ mice: *a*- to *b*-wave amplitude ratio demonstrating modest attenuation of *b*-wave amplitude for the *Slc4a5*$^{-/-}$ relative to wild-type mice. Wild-type mice have higher ratios compared with *Slc4a5*$^{-/-}$ mice showing that there is a small selective disruption of signal transmission from photoreceptor to bipolar retinal cells in *Slc4a5*$^{-/-}$ mice; *, $p < 0.05$.

Rod photoreceptor function, as indexed by the amplitude of the *a*-wave of the ERG (Fig. 7*D*), is reduced in *Slc4a5*$^{-/-}$ mice compared with WT controls. This finding is consistent with the observations on EM of diminished photoreceptor numbers in certain areas, shorter and dysmorphic outer segments, and inappropriate apposition of the photoreceptor outer segment tips with the RPE in *Slc4a5*$^{-/-}$ mice. Shown in Fig. 7*E* are the *b*-/*a*-wave amplitude ratios obtained from the ERG response to the brightest flash under dark-adapted conditions. The ERG *b*-wave originates from second-order neural cells present in the inner retina, and the *b*-/*a*-wave amplitude ratio is commonly used as an index of the relative performance of outer and middle retinal cells. In Fig. 7*E*, the *b*-/*a*-wave amplitude ratios for the mice are consistently lower than those for the wild-type controls, suggesting that in addition to the dysfunction observed at the level of the photoreceptors, there are also abnormalities either in signal transmission from photoreceptors to second-order neurons or in the second-order neural cells themselves.

The neurosensory retina of *Slc4a5*$^{-/-}$ mice exhibited multiple phenotypic abnormalities by light and electron microscopy. As shown in Fig. 8, *A* and *B*, NBCe2, which is normally localized in the outer plexiform layer in photoreceptor synaptic terminals, was not expressed in *Slc4a5*$^{-/-}$ mice. Both rod outer segments (ROS) and rod inner segments were shortened compared with the wild-type photoreceptor cells (Fig. 8, *C–E*). The nuclei in the proximal region of the outer nuclear layer (ONL) were disorganized, and the outer plexiform layer (OPL) was reduced in thickness, to the extent that cell nuclei from the ONL and inner nuclear layer were in close proximity. Compared with wild-type mice retina from *Slc4a5*$^{-/-}$ mice had varying degrees of retinal separation from the RPE (Fig. 8, *D* and *E*). Fig. 8*D* illustrates a retina with minimal separation showing a translucent zone between the apical region of the RPE and distal outer segments (ROS). Fig. 8*E* shows a retina where the neurosensory retina was completely detached from the RPE. In severely detached regions, there was evidence for photoreceptor cell degeneration, and macrophages were observed in the process of debris removal. Fig. 8, *F* and *G,* shows electron microscopy images of the retinal pigment epithelium/distal rod photoreceptor outer segment interface in wild-type and *Slc4a5*$^{-/-}$ mice. In wild-type retina, apical microvilli from the RPE, which normally interdigitate with distal ROS tips, are in close association with the apical surface of the RPE (Fig. 8*F*). In retina from *Slc4a5*$^{-/-}$ mice, apposition of distal ROS with the RPE was abnormal in that there was no interdigitation of these structures (Fig. 8*G*). This represents the translucent zone seen by light microscopy. Instead, RPE apical microvilli were densely packed in parallel, and the rod outer segment tips were displaced from the apical RPE plasma membrane by the length of the microvilli and showed disorganization of their membranous discs (Fig. 8*G*).

Recent studies have conjectured that an increased in the IOP-ICP difference can damage ganglion cells and the optic nerve (glaucoma phenotype) in the absence of an increase in IOP (normal tension glaucoma) (35). Our results are compatible with this hypothesis. Specifically, the measured IOP was not significantly different as follows: 18.8 ± 1.5 cm H_2O ($n = 5$) in wild-type mice *versus* 16.7 ± 1.0 cm H_2O ($n = 6$) in *Slc4a5*$^{-/-}$mice. However, given the observed differences in

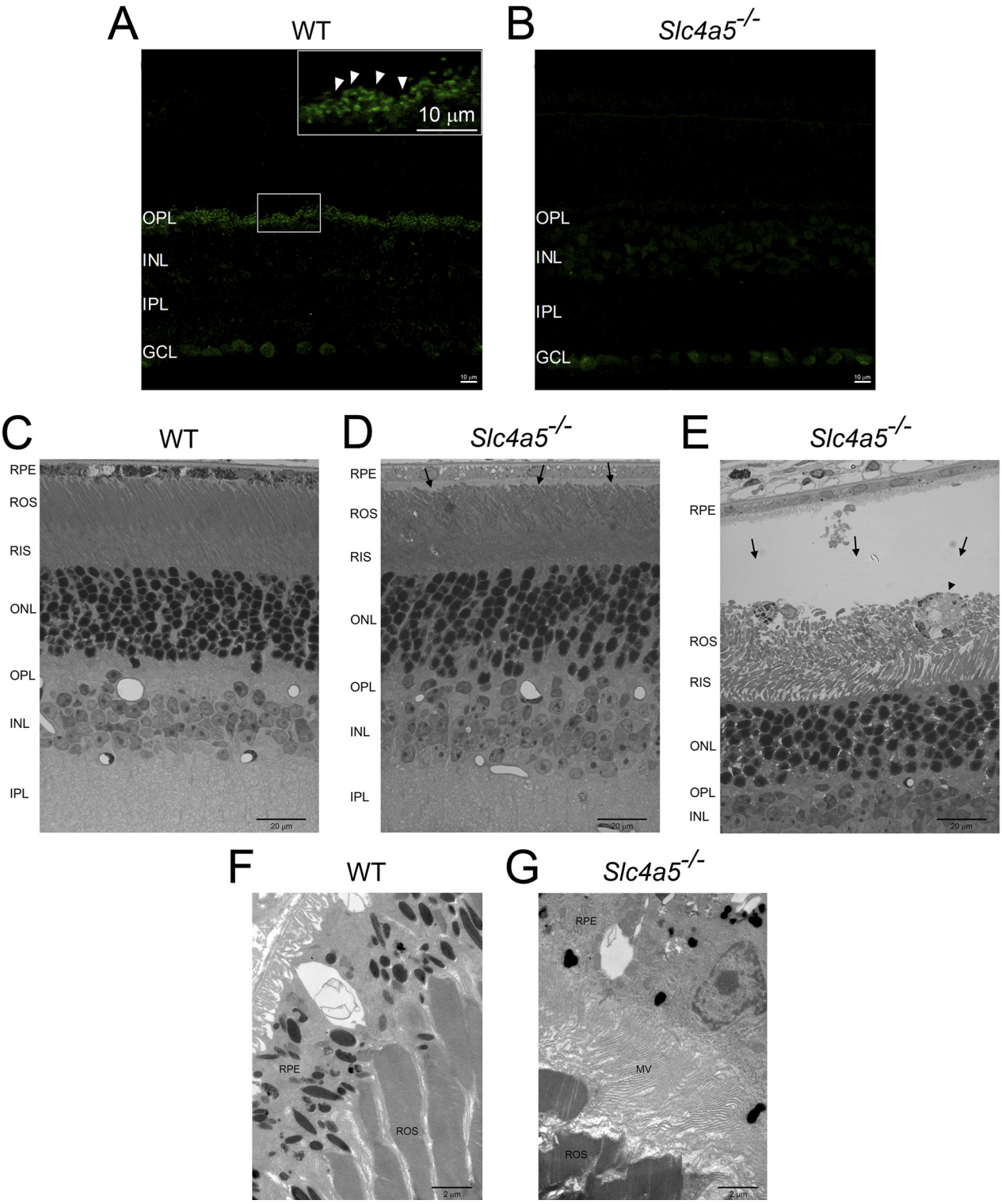

FIGURE 8. *A* and *B,* immunolocalization of *NBCe2* in the wild-type and *Slc4a5*$^{-/-}$ retina (*square box*). *A,* localization of NBCe2 in the OPL. *Inset*, higher magnification of a region in the OPL of wild-type mouse illustrates horseshoe-shaped ribbon-like structures (*arrowheads*) in the OPL that are absent in *Slc4a5*$^{-/-}$ mice (*B*). Faint nonspecific staining was detected in ganglion cells from both groups of mice. *OPL,* outer plexiform layer; *INL,* inner nuclear layer; *IPL,* inner plexiform layer; and *GCL,* ganglion cell layer. *Scale bar,* 10 μm. *C–E,* light microscopy of wild-type (*C*) and *Slc4a5*$^{-/-}$ retina (*D* and *E*). In *Slc4a5*$^{-/-}$ retina, a spectrum of abnormalities was detected. Some of the retina showed a translucent zone (*D*, *arrows*) between the apical region of the RPE and distal outer segments (ROS) that on electron microscopy is composed of densely pack RPE apical microvilli (*G*). The nuclei in the proximal region of the ONL are disorganized. A more severely affected retina is shown in *E* where a portion of the retina is detached (*arrows*) with photoreceptor cell death (reduced number of photoreceptor nuclei in the outer nuclear layer (*ONL*)). Large macrophages (*arrowhead*) are present among the damaged rod outer segments. *F* and *G,* electron microscopy of the retinal pigment epithelium/distal rod photoreceptor outer segment interface: wild-type (*F*) and *Slc4a5*$^{-/-}$ mice (*G*). Apical microvilli from the RPE of wild-type mice (*F*) interdigitate in close association with distal rod outer segment tips. The apical surface of the RPE in *Slc4a5*$^{-/-}$ mice (*G*) is displaced from distal rod outer segment tips by densely packed RPE apical microvilli (*MV*).

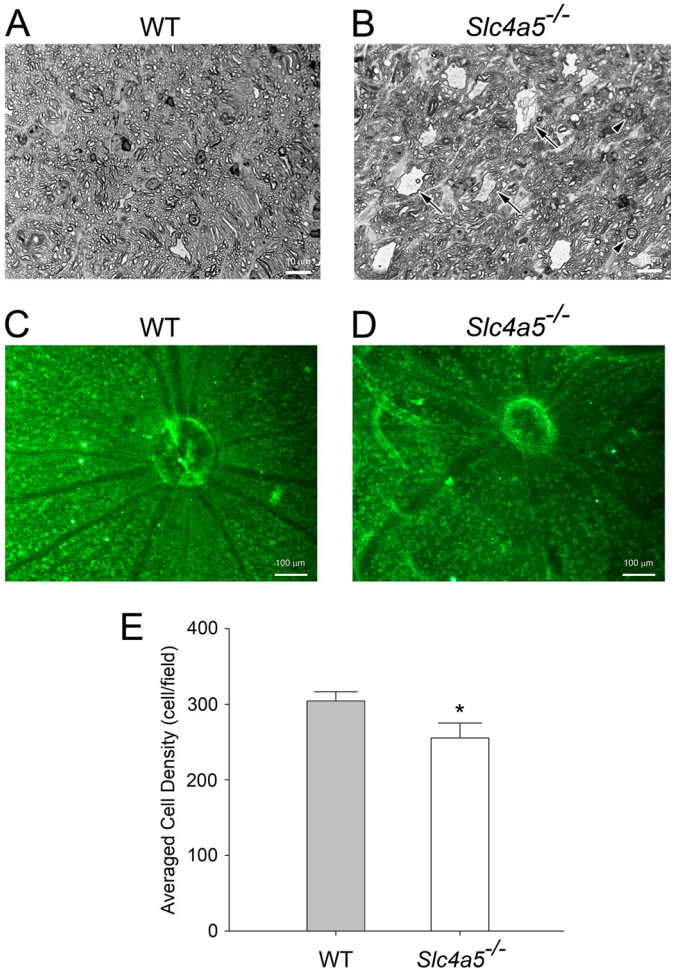

FIGURE 9. **Representative images of the optic nerve sections from wild-type (*A*) and *Slc4a5*$^{-/-}$ mice (*B*).** In *Slc4a5*$^{-/-}$ mice, large irregular axons (*arrows*) and condensed axons with degenerated myelin sheaths (*arrowheads*) were observed. *C* and *D,* RGCs in whole-mount retinas were labeled with antibodies against Rbpms. Representative images showing reduced RGC density in *Slc4a5*$^{-/-}$ mice (*D*) *versus* control (*C*). *E,* analysis of neuronal RGC density (averaged density) revealed a reduced number of RGCs in *Slc4a5*$^{-/-}$ retinas. The superior temporal and inferior temporal quadrants at 1.5 and 2.0 mm from the optic nerve head were most affected (not shown). *, $p < 0.05$.

ICP (Fig. 6), these values correspond to a significantly greater IOP-ICP gradient in *Slc4a5*$^{-/-}$ *versus* wild-type mice as follows: 13.7 ± 1.1 cm H_2O *versus* 9.6 ± 1.8 cm H_2O, respectively, $p < 0.05$. As shown in Fig. 9, *A* and *B, Slc4a5*$^{-/-}$ mice had optical nerve changes that included large irregular axons and condensed axons with degenerated myelin sheaths (Fig. 9, *A* and *B*). Analysis of neuronal RGC density revealed a reduced number of RGCs in *Slc4a5*$^{-/-}$ retinas (Fig. 9, *C*, *D*, and *E*).

DISCUSSION

The results demonstrate for the first time the fundamental biologic requirement for NBCe2 in maintaining neurologic structure and function. Mice lacking NBCe2 have a profound decrease in intracerebral volume and pressure associated with abnormal CSF electrolytes. Behaviorally, these mice are less sensitive to chemically induced (PTZ) seizures. In the absence of NBCe2, CPE cells have abnormalities in the localization of mitochondria, specific ion transporters (NCBE, NKCC1, and specific Na^+ pump subunits), and the cytoskeletal spectrin βII protein. These findings expand the biologic role of NBCe2 in CPE cells beyond merely its transport function and suggest that NBCe2 is involved in the modeling of CPE cells *in vivo*. We have previously reported that NBCe2 is expressed in the mammalian kidney and liver (36). In NBCe2$^{-/-}$ mice, the liver and kidney were grossly and histologically normal, as were the plasma electrolytes (not shown), suggesting that additional compensatory processes are present.

Given the function of NBCe2 as an electrogenic sodium bicarbonate cotransporter (17, 19), it is reasonable to speculate that the significant remodeling of CPE cells represents an array of compensatory changes because of an alteration in the activity (intracellular and/or extracellular) of Na^+, HCO_3^-, H^+, or membrane potential. Future studies are required to determine the exact molecular signaling mechanism(s) involved. Interestingly, a recent study showed that loss of the choroid plexus NCBE transporter resulted in basolateral rather than apical expression of NHE1 (28). This finding as well as the significant changes in the modeling of CPE cells due to loss of NBCe2 complements recent studies that have demonstrated that certain ion transporting proteins have additional important and unexpected roles in generating and maintaining the structural properties of epithelial cells and neurons. For example, in Zebrafish gut (37), Zebrafish brain ventricle (38), Zebrafish heart (39). and *Drosophila* trachea (40), the Na^+ pump is required for generating normal epithelial tubular structures. In *Caenorhabditis elegans* excretory cells, the EXC-4 (CLIC) chloride channel has an essential role in tubulogenesis and in preventing cyst formation (41). Local Na^+ ion levels altered by the pore-forming channel gramicidin can regulate the formation of tight junctional architecture (42). SKCa channel activation alters the fate of pluripotent cells toward cardiomyocyte specification (43). Calcium signals can alter neurotransmitter expression changing excitatory into inhibitory neurons (44). Changes in extracellular pH can alter the distribution of late endosomes in hippocampal neurons (45). Together, these examples suggest that local and/or compartmental changes in ion activity have very profound effects on cellular modeling. A deeper understanding of the involved pathways could potentially contribute to new therapeutic advances in the future.

Prior to this study, there have been no reported electrolyte measurements in CSF from mice presumably because of the technical difficulties involved with obtaining such measurements. The electrolyte content of CSF in mammals appears to be species-dependent (although technical measurement differences may account for some of the reported differences). In rats, the Na^+ concentration in CSF is ~150 meq/liter (46). The value of 162 meq/liter that we measured in wild-type mice approximates the value in cats (~160 meq/liter (47)). The CSF HCO_3^- concentration in rats is ~25 meq/liter (46), which approximates the value of 24 meq/liter reported in this study in wild-type mice. The value of 20 meq/liter in *Slc4a5*$^{-/-}$ mice with defective apical NBCe2-mediated sodium bicarbonate cotransport is the first demonstration that targeted disruption of a CPE transporter alters CSF chemistry. Although not currently practiced clinically, our findings certainly suggest the possibility that in the future measurements of ion chemistry

may have a diagnostic value in humans with mutations in specific CPE cell ion transporters.

In addition to the fundamental role played by NBCe2 in the maintenance of normal ventricular volume and intracranial pressure, our findings demonstrate the importance of NBCe2 in retinal biology. Previous studies have shown that maintenance of normal ion homeostasis in the retina is required to prevent retinal degeneration (48). In the synaptic terminal where NBCe2 is localized, PMCA1 and PMCA4 can mediate Ca^{2+}/H^+ exchange, which is a process that is pH-sensitive (49, 50). The activity of L-type voltage-gated Ca^{2+} channels in the synaptic terminus is also modulated by pH changes (51). It is therefore likely that NBCe2 plays an important role in buffering H^+ influx into the photoreceptor synaptic terminus. Abnormalities in retinal pH homeostasis because of loss of NBCn1 (*Slc4a7*) (52) and AE3 (*Slc4a3*) (53) cause retinal abnormalities in mice. Unlike electroneutral NBCn1 that is also localized to the photoreceptor synaptic terminus (52), NBCe2 transport (given its electrogenic nature) is predicted to be potentially sensitive to light-induced changes that modulate the photoreceptor inner segment membrane potential. Moreover, the retinal phenotype due to loss of NBCe2 is manifested by several unique features, including rod outer segment tip displacement from the apical RPE plasma membranes, shorter rod outer segments with disorganized membranous discs, densely packed RPE apical microvilli, detached neurosensory retina, and photoreceptor cell degeneration with macrophage infiltration. The finding that ganglion cell number was also decreased in number is in keeping with recent studies suggesting that an increase in the translaminar pressure differences (IOP-ICP pressure difference) can damage ganglion cells (glaucoma phenotype) even in the absence of an absolute increase in IOP due perhaps to changes in axonal transport or blood flow (35).

Although *Slc4a5*$^{-/-}$ mice are prone to developing retinal abnormalities, they are significantly more resistant to having chemically induced seizures. Mice with loss of NCBE (54) and aquaporin 4 (55) also have an increased seizure threshold. These transporters are expressed in neurons (29) and glia (56), respectively, throughout the brain, and the resistance to seizures has been attributed to decreased neuronal excitability. In contrast, NBCe2 is only expressed in CPE cells, where it mediates electrogenic sodium bicarbonate transport suggesting the possibility that changes in CSF dynamics and/or ion chemistry *per se* can reduce the propensity for chemically induced seizures in mammals. The loss of NBCe2 leads to decreased apical bicarbonate secretion and a decreased CSF bicarbonate concentration. Changes in CSF acid-base chemistry can potentially affect neuronal excitability (57). Given that CPE cell bicarbonate secretion is carbonic anhydrase-dependent (58), acetazolamide may function as an antiepileptic agent in part through this mechanism (33). The decrease in CSF K^+ concentration in *Slc4a5*$^{-/-}$ mice is also of potential pathophysiologic importance because modulation of the CSF K^+ concentration can significantly affect neuronal excitability (59). Altered CPE cell K^+ transport in *Slc4a5*$^{-/-}$ mice could result, for example, from a change in apical membrane potential (NBCe2 is electrogenic), the alteration in CSF acid-base chemistry, or via a remodeling of CPE cell K^+ transporters.

CSF production is altered in various disease states (6, 7). An understanding of the potential pathways involved has been aided by mammalian models of targeted disruption of specific CPE cell transporters in mice. It has previously been shown that aquaporin 1-deficient mice have decreased intracranial pressure (60), and aquaporin 4-deficient mice have decreased CSF production (61). Both aquaporin 1 and 4 expression were unchanged in NBCe2$^{-/-}$ CPE cells. In addition, mice with loss of CPE cell NCBE-mediated transport have decreased ventricular volume (54). Aquaporin 5 may play a role in developmental endolymph maturation in the inner ear (62), but it is not expressed in mouse brain (63). The finding that disruption of NBCe2 in mice significantly decreases intracranial pressure and ventricular volume highlights an important new mechanism for modulating CSF dynamics and CSF ion chemistry in mammals.

Acknowledgments—We acknowledge Karen Duff, Scott Fish, Andrew Frew, Harry Vinters, Cecilia Choi, and Eric A. Rosen for their technical assistance in various aspects of the experiments.

REFERENCES

1. Majumdar, D., and Bevensee, M. O. (2010) *Neuroscience* **171,** 951–972
2. Kahle, K. T., Simard, J. M., Staley, K. J., Nahed, B. V., Jones, P. S., and Sun, D. (2009) *Physiology* **24,** 257–265
3. Benfenati, V., and Ferroni, S. (2010) *Neuroscience* **168,** 926–940
4. Ryan, D. P., and Ptácek, L. J. (2010) *Neuron* **68,** 282–292
5. Lüscher, C., and Slesinger, P. A. (2010) *Nat. Rev. Neurosci.* **11,** 301–315
6. Johanson, C. E., Duncan, J. A., 3rd, Klinge, P. M., Brinker, T., Stopa, E. G., and Silverberg, G. D. (2008) *Cerebrospinal Fluid Res.* **5,** 10
7. Wolburg, H., and Paulus, W. (2010) *Acta Neuropathol.* **119,** 75–88
8. Poca, M. A., and Sahuquillo, J. (2005) *Expert Opin. Pharmacother.* **6,** 1525–1538
9. Foldvary-Schaefer, N., and Falcone, T. (2003) *Neurology* **61,** S2–S15
10. DeLellis, S. M. (2010) *J. Spec. Oper. Med.* **10,** 38–40
11. Praticò, D., Yao, Y., Rokach, J., Mayo, M., Silverberg, G. G., and McGuire, D. (2004) *J. Alzheimers Dis.* **6,** 385–449
12. Shuvaev, V. V., Laffont, I., Serot, J. M., Fujii, J., Taniguchi, N., and Siest, G. (2001) *Neurobiol. Aging* **22,** 397–402
13. Silverberg, G. D., Mayo, M., Saul, T., Rubenstein, E., and McGuire, D. (2003) *Lancet Neurol.* **2,** 506–511
14. Preston, J. E. (2001) *Microsc. Res. Tech.* **52,** 31–37
15. Damkier, H. H., Brown, P. D., and Praetorius, J. (2010) *Physiology* **25,** 239–249
16. Pushkin, A., Abuladze, N., Newman, D., Lee, I., Xu, G., and Kurtz, I. (2000) *Biochim. Biophys. Acta* **1493,** 215–218
17. Sassani, P., Pushkin, A., Gross, E., Gomer, A., Abuladze, N., Dukkipati, R., Carpenito, G., and Kurtz, I. (2002) *Am. J. Physiol. Cell Physiol.* **282,** C408–C416
18. Bouzinova, E. V., Praetorius, J., Virkki, L. V., Nielsen, S., Boron, W. F., and Aalkjaer, C. (2005) *Am. J. Physiol. Cell Physiol.* **289,** C1448–C1456
19. Millar, I. D., and Brown, P. D. (2008) *Biochem. Biophys. Res. Commun.* **373,** 550–554
20. Abuin, A., Hansen, G. M., and Zambrowicz, B. (2007) *Handb. Exp. Pharmacol.* 129–147
21. Joshi, M. A., Jeoung, N. H., Obayashi, M., Hattab, E. M., Brocken, E. G., Liechty, E. A., Kubek, M. J., Vattem, K. M., Wek, R. C., and Harris, R. A. (2006) *Biochem. J.* **400,** 153–162
22. Kong, W. C., and Cho, E. Y. (1999) *Life Sci.* **64,** 1773–1778
23. Kwong, J. M., Caprioli, J., and Piri, N. (2010) *Invest. Ophthalmol. Vis. Sci.* **51,** 1052–1058
24. Ishii, Y., Kwong, J. M., and Caprioli, J. (2003) *Invest. Ophthalmol. Vis. Sci.* **44,** 1982–1992

25. Shao, X. M., and Feldman, J. L. (2007) *J. Neurosci. Methods* **159,** 108–115
26. Wu, X. H., Ding, M. P., Zhu-Ge, Z. B., Zhu, Y. Y., Jin, C. L., and Chen, Z. (2006) *Neurosci. Lett.* **400,** 146–149
27. Lindsey, A. E., Schneider, K., Simmons, D. M., Baron, R., Lee, B. S., and Kopito, R. R. (1990) *Proc. Natl. Acad. Sci. U.S.A.* **87,** 5278–5282
28. Damkier, H. H., Prasad, V., Hübner, C. A., and Praetorius, J. (2009) *Am. J. Physiol. Cell Physiol.* **296,** C1291–C1300
29. Chen, L. M., Kelly, M. L., Rojas, J. D., Parker, M. D., Gill, H. S., Davis, B. A., and Boron, W. F. (2008) *Neuroscience* **151,** 374–385
30. Gao, B., Stieger, B., Noé, B., Fritschy, J. M., and Meier, P. J. (1999) *J. Histochem. Cytochem.* **47,** 1255–1264
31. González-Martínez, L. M., Avila, J., Martí, E., Lecuona, E., and Martín-Vasallo, P. (1994) *Biol. Cell* **81,** 215–222
32. Praetorius, J., and Nielsen, S. (2006) *Am. J. Physiol. Cell Physiol.* **291,** C59–C67
33. Reiss, W. G., and Oles, K. S. (1996) *Ann. Pharmacother.* **30,** 514–519
34. Newton, P. N., Thai le, H., Tip, N. Q., Short, J. M., Chierakul, W., Rajanuwong, A., Pitisuttithum, P., Chasombat, S., Phonrat, B., Maek-A-Nantawat, W., Teaunadi, R., Lalloo, D. G., and White, N. J. (2002) *Clin. Infect. Dis.* **35,** 769–772
35. Ren, R., Jonas, J. B., Tian, G., Zhen, Y., Ma, K., Li, S., Wang, H., Li, B., Zhang, X., and Wang, N. (2010) *Ophthalmology* **117,** 259–266
36. Abuladze, N., Pushkin, A., Tatishchev, S., Newman, D., Sassani, P., and Kurtz, I. (2004) *Am. J. Physiol. Cell Physiol.* **287,** C781–C789
37. Bagnat, M., Cheung, I. D., Mostov, K. E., and Stainier, D. Y. (2007) *Nat. Cell Biol.* **9,** 954–960
38. Lowery, L. A., and Sive, H. (2005) *Development* **132,** 2057–2067
39. Shu, X., Cheng, K., Patel, N., Chen, F., Joseph, E., Tsai, H. J., and Chen, J. N. (2003) *Development* **130,** 6165–6173
40. Paul, S. M., Ternet, M., Salvaterra, P. M., and Beitel, G. J. (2003) *Development* **130,** 4963–4974
41. Berry, K. L., Bülow, H. E., Hall, D. H., and Hobert, O. (2003) *Science* **302,** 2134–2137
42. Rajasekaran, S. A., Palmer, L. G., Moon, S. Y., Peralta Soler, A., Apodaca, G. L., Harper, J. F., Zheng, Y., and Rajasekaran, A. K. (2001) *Mol. Biol. Cell* **12,** 3717–3732
43. Kleger, A., Seufferlein, T., Malan, D., Tischendorf, M., Storch, A., Wolheim, A., Latz, S., Protze, S., Porzner, M., Proepper, C., Brunner, C., Katz, S. F., Varma Pusapati, G., Bullinger, L., Franz, W. M., Koehntop, R., Giehl, K., Spyrantis, A., Wittekindt, O., Lin, Q., Lin, Q., Zenke, M., Fleischmann, B. K., Wartenberg, M., Wobus, A. M., Boeckers, T. M., and Liebau, S. (2010) *Circulation* **122,** 1823–1836
44. Marek, K. W., Kurtz, L. M., and Spitzer, N. C. (2010) *Nat. Neurosci.* **13,** 944–950
45. Parton, R. G., Dotti, C. G., Bacallao, R., Kurtz, I., Simons, K., and Prydz, K. (1991) *J. Cell Biol.* **113,** 261–274
46. Reed, D. J., Withrow, C. D., and Woodbury, D. M. (1967) *Exp. Brain Res.* **3,** 212–219
47. Vogh, B. P., and Maren, T. H. (1975) *Am. J. Physiol.* **228,** 673–683
48. Krizaj, D., and Copenhagen, D. R. (2002) *Front. Biosci.* **7,** d2023–d2044
49. Krizaj, D., Demarco, S. J., Johnson, J., Strehler, E. E., and Copenhagen, D. R. (2002) *J. Comp. Neurol.* **451,** 1–21
50. Trapp, S., Lückermann, M., Kaila, K., and Ballanyi, K. (1996) *Neuroreport* **7,** 2000–2004
51. Barnes, S., Merchant, V., and Mahmud, F. (1993) *Proc. Natl. Acad. Sci. U.S.A.* **90,** 10081–10085
52. Bok, D., Galbraith, G., Lopez, I., Woodruff, M., Nusinowitz, S., Beltrandel-Rio, H., Huang, W., Zhao, S., Geske, R., Montgomery, C., Van Sligtenhorst, I., Friddle, C., Platt, K., Sparks, M. J., Pushkin, A., Abuladze, N., Ishiyama, A., Dukkipati, R., Liu, W., and Kurtz, I. (2003) *Nat. Genet.* **34,** 313–319
53. Alvarez, B. V., Gilmour, G. S., Mema, S. C., Martin, B. T., Shull, G. E., Casey, J. R., and Sauvé, Y. (2007) *PLoS One* **2,** e839
54. Jacobs, S., Ruusuvuori, E., Sipilä, S. T., Haapanen, A., Damkier, H. H., Kurth, I., Hentschke, M., Schweizer, M., Rudhard, Y., Laatikainen, L. M., Tyynelä, J., Praetorius, J., Voipio, J., and Hübner, C. A. (2008) *Proc. Natl. Acad. Sci. U.S.A.* **105,** 311–316
55. Binder, D. K., Oshio, K., Ma, T., Verkman, A. S., and Manley, G. T. (2004) *Neuroreport* **15,** 259–262
56. Nielsen, S., Nagelhus, E. A., Amiry-Moghaddam, M., Bourque, C., Agre, P., and Ottersen, O. P. (1997) *J. Neurosci.* **17,** 171–180
57. Xiong, Z. Q., Saggau, P., and Stringer, J. L. (2000) *J. Neurosci.* **20,** 1290–1296
58. Saito, Y., and Wright, E. M. (1982) *J. Physiol.* **328,** 229–243
59. Pedley, T. A., Zuckermann, E. C., and Glaser, G. H. (1969) *Exp. Neurol.* **25,** 207–219
60. Oshio, K., Watanabe, H., Song, Y., Verkman, A. S., and Manley, G. T. (2005) *FASEB J.* **19,** 76–78
61. Li, X., Kong, H., Wu, W., Xiao, M., Sun, X., and Hu, G. (2009) *Neuroscience* **162,** 67–77
62. Merves, M., Krane, C. M., Dou, H., Greinwald, J. H., Menon, A. G., and Choo, D. (2003) *J. Assoc. Res. Otolaryngol.* **4,** 264–275
63. Papadopoulos, M. C., Manley, G. T., Krishna, S., and Verkman, A. S. (2004) *FASEB J.* **18,** 1291–1293